Dynamical Aspects of Isomerization and Melting Transitions in [H₂O]₈[†]

Daniel Laria,[‡,¶] Javier Rodriguez,[‡] Christoph Dellago,[§] and David Chandler*,[⊥]

*Unidad Actividad Química, Comisión Nacional de Energía Atómica, Avenida Libertador 8250,
1429 Capital Federal, Argentina; Departamento de Química Inorgánica, Analítica e Química-Física e
INQUIMAE, Facultad de Ciencias Exactas y Naturales, Universidad de Buenos Aires, Ciudad Universitaria,
Pabellón II, 1428, Capital Federal, Argentina; Department of Chemistry, University of Rochester, Rochester,
New York 14627; and Department of Chemistry and Kenneth S. Pitzer Center for Theoretical Chemistry,
University of California, Berkeley, California 94720*

We present a transition path sampling study of the dynamics of isomerization between the S_4 and the D_{2d} cubic structures of the water octamer. The reaction mechanism involves a transition state characterized by a distorted face exhibiting a diagonal hydrogen bond. Analysis of an ensemble of trajectories shows that the isomerization requires concerted flips of double proton donor molecules and the interchange between dangling and bonding hydrogens in single proton donor molecules. At a total energy $E = -60.5$ kcal/mol, we calculated that the characteristic time for the interconversion is of the order of milliseconds. We have also investigated pathways for the melting transition at temperatures $T \approx 200$ K. We find that the barrier for solid–liquid interconversions never exceeds $2k_BT$ measured from the liquid side. Such transitions between liquid and solid do not involve the passage over an energetic barrier; instead, the stabilization of the liquid phase is the result of a cancellation between energetic and entropic contributions.

I. Introduction

Clusters with sizes in the nanometer scale are normally considered as intermediate entities between bulk matter and isolated molecules. From a thermodynamic point of view, clusters are inherently metastable since the most stable configurations for a handful of particles within a macroscopic volume in contact with a heat reservoir correspond to fully evaporated states. However, one may extract thermodynamically relevant information, if clusters survive sufficiently long compared to microscopic relaxation times.

At low enough temperatures, clusters exhibit solidlike behavior. Under these conditions, their structural and dynamical features do not differ substantially from those of polyatomic molecules: fluctuations of interparticle distances much smaller than their average values and a dynamics characterized by small amplitude vibrations. Depending on interparticle interactions and size, molecular solid clusters may exhibit a manifold of stable structures. As one moves to higher temperatures, but before evaporation becomes important, there is typically a thermal interval where cluster structures look similar to portions of amorphous liquidlike bulk phases. Perhaps, the most clear manifestation of the liquidlike regime is the presence of intracluster diffusion. While the melting temperature of bulk phases is well-defined, interconversions between solid–liquid structures in clusters take place spontaneously over an interval of temperatures.[1–7]

At present, there is unambiguous experimental evidence of the existence of solid and liquidlike clusters;[8–11] however, the vast majority of the microscopic details characterizing both environments comes from computer simulations. Melting transitions can be localized either by determining the slope of the energy vs temperature curve or by computing relative fluctuations in the interparticle distances.[1,12] In many cases, well below the melting temperature, a second kind of structural transformation involving two different stable solidlike structures may also occur. The present paper examines dynamical aspects of these two different kinds of structural transitions, both taking place in the water octamer.

The first process is the isomerization between the S_4 and D_{2d} solid cubic structures characterized by different connectivity patterns of the hydrogen bonds. Recently, these two stable structures have been identified in infrared experiments on isolated water clusters[13] and in experiments involving benzene attached to the water octamer.[14] Second, we investigated dynamical pathways for the melting transition of the octamer. Although there is a large body of investigations devoted to the study of structures of small solid and liquid aqueous clusters,[15–24] very little is known about the dynamics and the mechanisms that drive the interconversion between them.

Our methodology relies on the recently developed path sampling method.[26–29] This approach not only provides a route to the computation of rate constants but also allows the characterization of reactive channels and transition states.[30] In contrast to other methods based on biased or constrained dynamics,[31] this new methodology does not require an a priori definition of a reaction coordinate that may preclude proper sampling of all relevant fluctuations governing the dynamics of the reactive process. Instead, it is based on harvesting bias-free reactive pathways joining reactant and product states by sampling appropriate probability distributions of trajectories.

This work is organized as follows: in section II we present some relevant details about the model we adopted and a brief

description of the transition path sampling method. Results for isomerization dynamics of [H$_2$O]$_8$ are presented in section III. The melting transition is analyzed in section IV.

II. Methods

A. Molecular Dynamics. All trajectories were generated using classical molecular dynamics.[32] Water−water interactions were modeled using the TIP4P potential.[33] This model yields reasonable estimates for the energetics and stable structures of the water dimer and other small water clusters as well.[16] All simulations were performed at constant energy with vanishing total linear and angular momentum. The velocity version of the Verlet algorithm[32] was used to integrate the equations of motion with a time steps of 1 fs. To handle intramolecular constraints in the water molecules, the RATTLE[34] algorithm was implemented.

B. Reaction Rate Constants from Transition Path Sampling. Consider the isomerization between two stable states $\mathcal{A}$ and $\mathcal{B}$

$$\mathcal{A} \xrightarrow{k} \mathcal{B}$$

The rate constant k of the reaction is related to the long time behavior of the correlation function

$$C(t) = \frac{\langle h_A(0)h_B(t)\rangle}{\langle h_A\rangle} \tag{1}$$

Here, $h_A(t)$ is unity if the system is at the stable state $\mathcal{A}$ at time t and zero otherwise, and $h_B(t)$ is defined analogously. Angular brackets, $\langle ... \rangle$, denote equilibrium ensemble averages. If there is a separation between the time scales characterizing the reactive process τ_{reac} and other microscopic processes τ_{mic}, the function $C(t)$ reaches linear behavior after a short transient

$$C(t) \approx kt \qquad \tau_{\text{mic}} \ll t \ll \tau_{\text{reac}} \tag{2}$$

from which it is possible to extract the rate constant k.

In the transition path sampling method, the time correlation function $C(t)$ is calculated from an average taken over an ensemble of reactive trajectories of time length $\mathcal{T}$. Various Monte Carlo procedures have been devised to generate a properly weighted set of pathways.[26−28]

A convenient factorization of $C(t)$ can be introduced,[29] namely

$$C(t) = \langle h_B(t)\rangle_{AB} \times \frac{C(t')}{\langle h_B(t')\rangle_{AB}} \tag{3}$$

where t' is an arbitrary time between 0 and $\mathcal{T}$. In eq 3, the "path average" $\langle h_B(t)\rangle_{AB}$ is given by

$$\langle h_B(t)\rangle_{AB} = \frac{\langle h_A(0)h_B(t)H_B(\mathcal{T})\rangle}{\langle h_A(0)H_B(\mathcal{T})\rangle} \tag{4}$$

where the function $H_B(\mathcal{T})$ is unity if the system reaches state $\mathcal{B}$ at any time t within the time interval [0, $\mathcal{T}$] and zero otherwise. That is

$$H_B(\mathcal{T}) \equiv \max_{0 \le t \le \mathcal{T}} h_B(t) \tag{5}$$

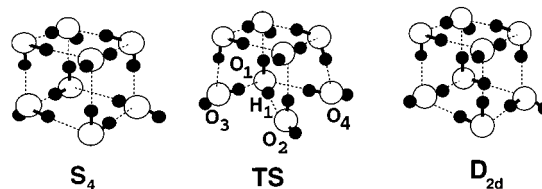**Figure 1.** S_4 and D_{2d} structures for the [H$_2$O]$_8$. Also shown is a typical transition state for transitions between these two structures with the molecular labeling described in section III.B.

The rate constant can be computed from the plateau value of the time derivative $\dot{C}(t)$:

$$k = \dot{C}(t) = \langle \dot{h}_B(t)\rangle_{AB} \times \frac{C(t')}{\langle h_B(t')\rangle_{AB}}, \quad \tau_{\text{mic}} \ll t \ll \tau_{\text{reac}} \tag{6}$$

Further details on how to implement the calculation of the two factors in eq 3 can be found in ref 29.

III. [H$_2$O]$_8$ Isomerization

A. Reaction Rates. Stable cubic S_4 and D_{2d} structures of the water octamer are shown in Figure 1. Both isomers present hydrogen bond connectivities characterized by four double proton donor−single proton acceptor (DDA) molecules bonded to four single proton donor−double proton acceptor (DAA) molecules. Interconversions between these two structures require flipping the four hydrogen bonds lying on the base of the cube. Precise quantum calculations[35] show that the S_4 isomer is slightly more stable ($\Delta E \approx -0.05$ kcal/mol) than the D_{2d} one.[36] At $E \approx -55$ kcal/mol, spontaneous transitions between the two TIP4P cubic forms occur at typical time intervals of 1−2 ns.

The path sampling procedure to determine the rate of isomerization k_{iso} requires a proper definition of an order parameter ξ that unambiguously identifies stable D_{2d} and S_4 regions of phase space. Guided by the direct inspection of trajectories that included several episodes of such interconversions, we focused our attention on one of the cube faces and defined an order parameter based on angular variables associated with the coplanar hydrogen bond of one particular DDA molecule, hereafter referred to as molecule 1. To clarify our notation, in what follows the four relevant DDA and DAA waters participating in the interconversion will be denoted as $i = 1, 2$ and $i = 3, 4$, respectively. The order parameter was chosen according to

$$\xi = \cos(\phi_2) - \cos(\phi_1) \tag{7}$$

where $\cos(\phi_i)$ is defined in terms of the following scalar product

$$\cos(\phi_i) = \frac{\mathbf{r}_{H_1O_1} \cdot \mathbf{r}_{O_jO_1}}{|\mathbf{r}_{H_1O_1}||\mathbf{r}_{O_jO_1}|} \tag{8}$$

where $j = 3, 4$ for $i = 1, 2$, respectively (see snapshot B in Figure 4). In eq 8, $\mathbf{r}_{\alpha_i\gamma_j} = \mathbf{r}_i^\alpha - \mathbf{r}_j^\gamma$, where $\mathbf{r}_i^\alpha$ denotes the position of site α in the ith molecule. With this definition, we characterized S_4 structures by $\xi \le -0.85$ and D_{2d} structures by $\xi \ge 0.85$.

Figure 2 shows the time evolution of ξ along a typical reactive path of time length $\mathcal{T} = 8$ ps, computed at a total energy $E = -60.5$ kcal/mol. Note that the passage from S_4 to D_{2d} structures includes an intermediate stage lasting of the order of 1.5 ps, during which the order parameter remains close to zero. During that period, there are large distortions in the original connectivity pattern in one of the cube faces that exhibits two broken hydrogen bonds and a new bond along the diagonal that joins
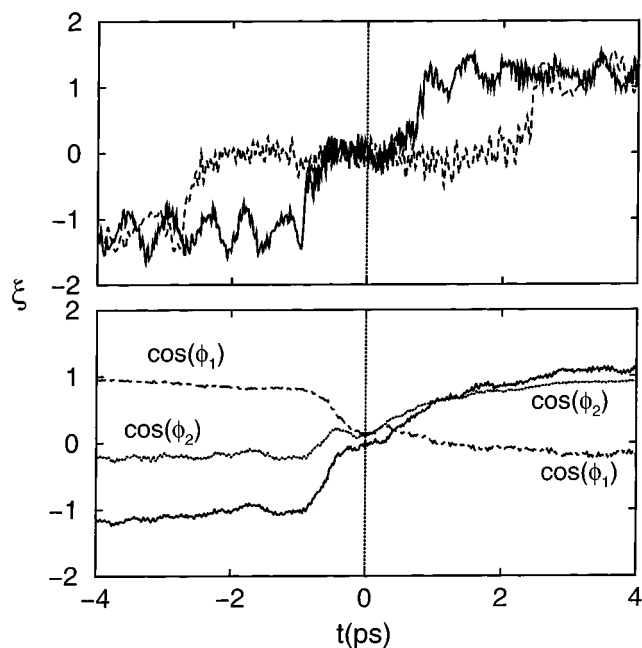
Figure 2. Top panel: Time evolution of $\xi(t)$ for a representative trajectory at $E = -60.5$ kcal/mol (solid line) and $E = -63$ kcal/mol (dashed line). Bottom panel: Relaxation of the order parameter for the $S_4 \rightarrow D_{2d}$ interconversion of $[H_2O]_8$ at $E = -60.5$ kcal/mol. Also shown the relaxations of the angular variables $\cos(\phi_i)$ (see text).
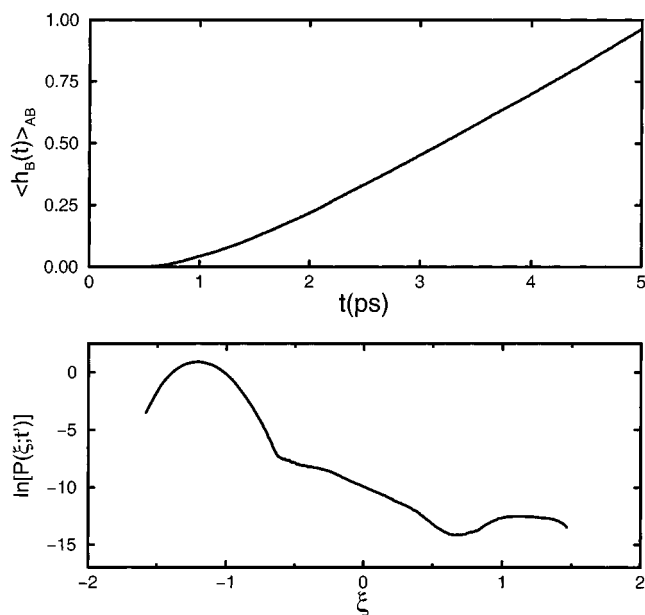

Figure 3. Top panel: Path average $\langle h_B(t)\rangle_{AB}$ for the $S_4 \rightarrow D_{2d}$ interconversion of $[H_2O]_8$ at $E = -60.5$ kcal/mol. Bottom panel: Probability distribution $P(\xi;t')$ (see text) for the same interconversion.

the two original DDA molecules (see structure TS in Figure 1). A structure with similar characteristics has been already reported as a secondary minimum lying approximately 2 kcal/mol above the global minimum of the cubic octamer in ref 23. A similar inspection of a lower energy trajectory computed at $E = -63$ kcal/mol also shown in the top panel of Figure 2, reveals that the residence time in this intermediate state increases up to ≈ 6 ps. This time interval much longer than τ_{mic} suggests that the interconversion at low energies proceeds via a two step "reaction" mechanism, including a marginally stable intermediate state characterized by a diagonal hydrogen bond.

Using the transition path sampling method, we have computed the rate constant for the $S_4 \rightarrow D_{2d}$ interconversion at $E = -60.5$
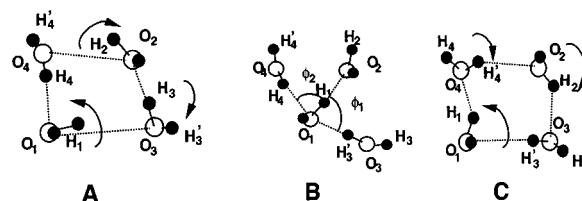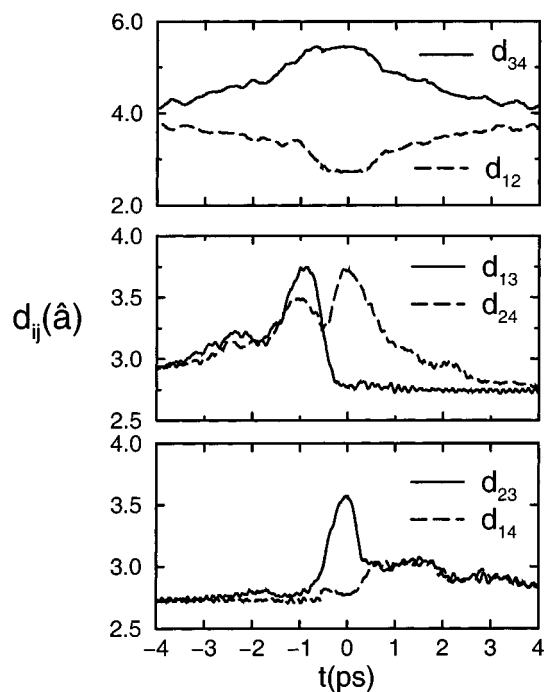

Figure 4. Relaxation of several O−O distances (in Å) for the $S_4 \rightarrow D_{2d}$ interconversion of $[H_2O]_8$ at $E = -60.5$ kcal/mol. Also shown typical instantaneous configurations of the relevant face of the cube $t = -1$ ps (A); $t = 0$ ps (B) and $t = 1$ ps (C).

kcal/mol. Accordingly, the corresponding transition path ensemble consists of all pathways starting from phase space points with $E = -60.5$ kcal/mol located in region S_4 and reaching region D_{2d} within 5 ps. Results for $\langle h_B(t)\rangle_{AB}$ ($A = S_4$, $B = D_{2d}$) are shown in the top panel of Figure 3; the linear regime that characterizes the time scale separation is attained after an initial transient of ≈ 4 ps. To compute the time-independent portion of eq 5, we first calculated $P(\xi';t')$ defined as

$$P(\xi';t') = \frac{\langle h_A \delta(\xi(t') - \xi')\rangle}{\langle h_A \rangle} \qquad (9)$$

where $\xi(t')$ is the value of the order parameter at time t'. $C(t')$ can then be expressed as

$$C(t') = \int_{\xi_{min}}^{\xi_{max}} P(\xi;t')\, d\xi \qquad (10)$$

where ξ_{min} and ξ_{max} represent the boundaries of the order parameter interval that characterize the stable D_{2d} product state. Results for $P(\xi';t')$ for $t' = 4$ ps are shown in the bottom panel of Figure 3; the curve was constructed using the umbrella sampling procedure described in ref 29 by matching five histograms spanning the following intervals of the order parameter: $\xi \leq -0.75$; $-0.9 \leq \xi \leq -0.2$; $-0.3 \leq \xi \leq 0.3$; $0.2 \leq \xi \leq 0.9$; and $\xi \geq 0.75$. The two local maxima $P(\xi,t)$ correspond to the two long-lived stable states between which the transition occurs. The resulting value of $C(t') = \int_{0.85}^{\infty} P(\xi;t')\, d\xi = 2.1 \times 10^{-6}$ yields an interconversion rate of $k = 5 \times 10^4$ s^{-1}.
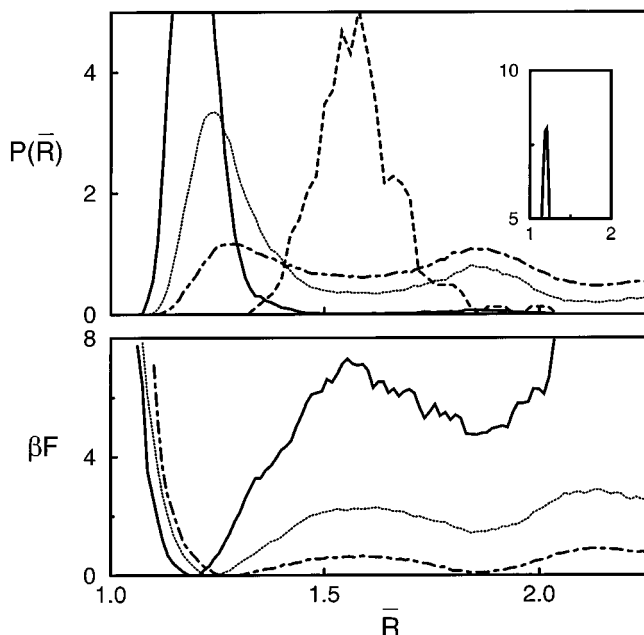
Figure 5. Top panel: probability distribution $P[\bar{R}]$ for the order parameter $\bar{R}$ at different energy values. $E = -55$ kcal/mol (solid line); $E = -50.5$ kcal/mol (dotted line); $E = -48$ kcal/mol (dot−dashed line). Also shown the transition state distribution of the order parameter at $E = -50.5$ kcal/mol (dashed line). Bottom panel: Free energy profiles for the order parameter. Same labeling as in the top panel. All curves were brought to zero at their respective minima.

B. Reaction Mechanism. The analysis of a large number of reactive trajectories permits the characterization of an ensemble of transitions states. A configuration on a reactive trajectory is defined to be a transition state if trajectories initiated at that configuration with random initial momenta have equal probability to reach either stable state after a certain transient time that we set to 2 ps. We analyzed sets of 50 trajectories for each trial initial configuration. Once a transition state was identified in each trajectory, we computed relaxation profiles of different physical observables by aligning the ensemble of reactive paths so that the their time origins coincide at their transition states.

The qualitative characteristics depicted in the single trajectory of Figure 2 coincide with those observed from the study of an ensemble of temporally aligned reactive paths. In the bottom panel of that figure, we present results for the relaxation of the order parameter and the angular variables $\cos(\phi_i)$ obtained from an ensemble of 150 trajectories. Note that transition states are characterized by $\langle\cos(\phi_i)\rangle_{\mathcal{TS}}$ ($i = 1, 2$) close to ≈ 0.12, yielding $\langle\xi\rangle_{\mathcal{TS}} \approx 0$, where $\langle...\rangle_{\mathcal{TS}}$ denotes an average taken from the set of trajectories at their respective transition state.

The complementary analysis of relaxation of several interatomic distances $d_{ij} = |\mathbf{r}_{O_iO_j}|$ is helpful to unveil details of the mechanisms and the structural transformations that take place along the interconversion.

The results presented in Figure 4 indicate that the transformation proceeds according to the following sequence: (i) a gradual enlargement/reduction of the distances d_{12} and d_{34} involving pairs of DAA and DDA molecules (see top panel of Figure 4); (ii) at $t \approx -1$ ps, the hydrogen bonds between pairs (1,3) and (2,4) break down (see middle panel and snapshot A of Figure 5); (iii) during the next picosecond, the hydrogen bond between the pair (1,3) is recovered via H$'_3$ (see snapshot B). At the same time, a diagonal hydrogen bond is established between the molecules 1 and 2; note that only the former molecule retains its DDA character since molecule 2 exhibits a dangling hydrogen H$_2$. The transition state is characterized by $d_{12} \approx d_{13} \approx d_{14} \approx$

2.75 Å and $\phi_1 \approx \phi_2 \approx 83°$. The deactivation from the transition state into products proceeds by three sequential flips (see snapshot C): (iv) molecule 2 recovers its DDA status by rotating its dangling hydrogen H$_2$ toward molecule 3; (v) a rotation of molecule 4 restores its bond with molecule 2 via H$'_4$; and (vi) a final rotation of molecule 2 establishes the connectivity with molecule 4. Summarizing, the overall interconversion mechanism can be formulated in terms of two in-plane rotations of hydrogens of DDA molecules, with amplitudes 90° inward (H$_1$) and 270° outward (H$_2$) and two rotations of DAA molecules with an interchange in the original status of their hydrogens as donor/dangling atoms (H$_i$ ↔ H$'_i$, for $i = 3, 4$).

IV. Melting Pathways

Solid ($\mathcal{S}$)−liquid ($\mathcal{L}$) transitions in the water octamer have been extensively studied by Wales et al.[19] Phase coexistence was investigated not only in terms of structural and energetic criteria but also by analyzing short-time averages of the total kinetic energy. The presence of a bimodal profile in the histograms of the temporally averaged kinetic energy revealed the alternation of liquidlike and solidlike episodes along the length of the simulation experiments. The melting transition for the TIP4P octamer was located at a total energy close to $E \approx -50$ kcal/mol, which corresponds to a temperature $T_m \approx 190$ K.

In a similar spirit, we considered temporally averages of different observables $\mathcal{Q}(t)$ computed as

$$\bar{\mathcal{Q}}(t) = \frac{1}{2\tau_0} \int_{t-\tau_0}^{t+\tau_0} \mathcal{Q}(t')\,\mathrm{d}t' \qquad (11)$$

Instead of resorting to an energetic criterion to determine whether an instantaneous configuration could be ascribed to either a solid or a melted structure, we found it more appropriate to choose a structural order parameter $\bar{R}(t)$, where $R(t)$ is the ratio between the biggest and smallest moments of inertia of the cluster at time t. The direct analysis of several melting transitions revealed that liquid clusters exhibit rather asymmetric structures with values of $\bar{R}$ much larger than those corresponding to a cubic shape, where $\bar{R} \simeq 1$. In the top panel of Figure 5 we show three histograms for the order parameter at the vicinity of the melting transition collected during rather long 10 ns simulations with $\tau_0 = 0.5$ ps. Also shown in Figure 5 is distribution of the order parameter in the transition path ensemble (dashed line). $\mathcal{S}$ and $\mathcal{L}$ structures can be roughly characterized by $\bar{R}_{\mathcal{S}} \approx 1.25$ and $\bar{R}_{\mathcal{L}} \approx 1.8$, respectively.

Furthermore, a thermodynamic interpretation of these results can be obtained by considering the free energy $F(\bar{R})$ defined by

$$\beta_m F(\bar{R}) = -\ln P(\bar{R}) \qquad (12)$$

where $P(\bar{R})$ is the probability distribution of $\bar{R}$. β_m^{-1} is Boltzmann constant times a temperature of the order of T_m. The free energy profiles are depicted in the bottom panel of Figure 5 where we clearly see that $\mathcal{S} \rightarrow \mathcal{L}$ transitions present small free energy activation barriers located at $\xi_{\mathcal{TS}} \approx 1.55$, which never surpass $2k_BT_m$, measured from the liquid side. Accordingly, the solid−liquid interconversions will not be characterized by a clear time scale separation between τ_{mic} and τ_{reac}, precluding the possibility of describing the kinetics of melting with a simple rate constant.

Yet, one can still exploit the idea of sampling over an ensemble of reactive paths to gain further insight about the mechanisms that drive the melting transitions. To that end, we
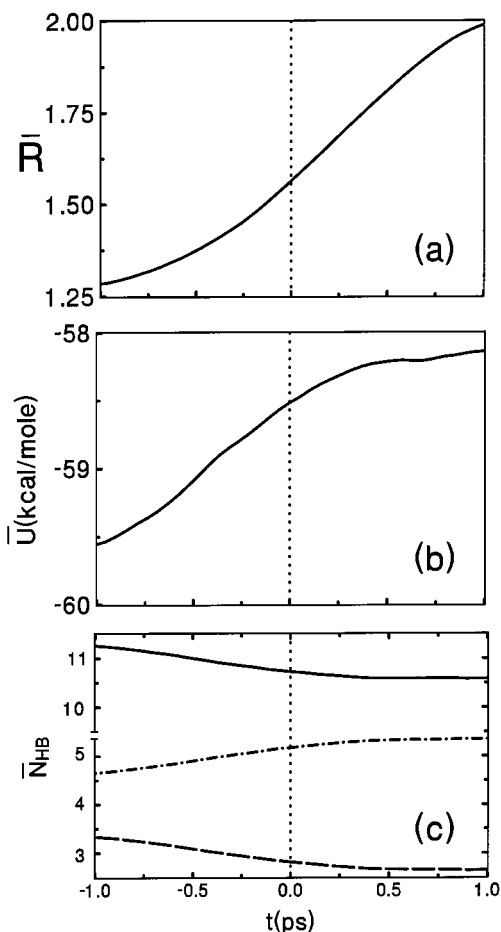
2650 *J. Phys. Chem. A, Vol. 105, No. 12, 2001*

Laria et al.

Figure 6. Relaxation of several relevant observables for the melting transition of $[H_2O]_8$ at $E = -50.5$ kcal/mol: (a) $\bar{R}$, (b) time average of the potential energy, and (c) time averages of the number of hydrogen bonds (solid line), single donors (dot-dashed line) and double donors (dashed line).

considered an ensemble of 200 statistically independent reactive paths at a total energy $E = -50.5$ kcal/mol. These pathways are separated by 50 successful "shooting" moves.[29] In each of these paths, we searched for transition states according to the 50%−50% dynamic probabilistic criterion described in section III.B and computed relaxation profiles for several temporally averaged observables of interest during a short 2 ps time interval to reduce the effect of recrossings of the transition states. Relaxation results for $\bar{R}(t)$ and $\bar{U}(t)$, where U is the total potential energy of the cluster, are shown in Figure 6. The collection of transition states are characterized by average values $\langle \bar{R} \rangle_{\mathcal{TS}} = 1.56$ and $\langle \bar{U} \rangle_{\mathcal{TS}} = -58.5$ kcal/mol. Incidentally, the fact that the distribution of $\bar{R}_{\mathcal{TS}}$ (also shown in the top panel of Figure 5) is concentrated around the location of the free energy barrier obtained from a previous equilibrium run also suggests that the geometrical order parameter can be considered as a reasonable reaction coordinate to describe the melting transition.

More interestingly, we found that the time evolution of the relaxation of $\bar{U}(t)$ shows a monotonic behavior with no energetic barrier separating solid from liquid structures.

An equivalent description of this feature can be cast in terms of the time evolution of the number of hydrogen bonds in the octamer during the melting process. To define a hydrogen bond, we adopted a geometrical criterion similar to that described in ref 25, and set the threshold O−O distance and hydrogen bond angle at 3.6 Å and 30°, respectively. In the bottom panel of Figure 6 we have included path averages of the time evolution of the total number of hydrogen bonds, discriminating contributions from single and double donor molecules. We see that the melting transitions involve a gradual reduction from 11.3 down to 10.6 hydrogen bonds, which is the result of a gain of 0.7 single donor molecules and a similar loss of double donor molecules. Moreover, the passage over the different transition states does not include intermediate structures with a lesser extent of hydrogen-bond connectivity. This suggests that the liquid state is stabilized by an entropy increase related to the breaking of hydrogen bonds and associated increase in disorder.

References and Notes

(1) Jellinek, J.; Beck, T. L.; Berry R. S. *J. Chem. Phys.* **1986**, *84*, 2783. Beck, T. L.; Jellinek, J.; Berry, R. S. *J. Chem. Phys.* **1987**, *87*, 545. Beck, T. L.; Berry, R. S. *J. Chem. Phys.* **1988**, *88*, 3910.

(2) Berry, R. S.; Beck, T. L.; Davis, H. L.; Jellinek, J. *Adv. Chem. Phys.* **1988**, *70B*, 75.

(3) Berry R. S.; Wales, D. J. *Phys. Rev. Lett.* **1989**, *63*, 1156. Berry, R. S.; Wales, D. J. *J. Chem. Phys.* **1990**, *92*, 4308.

(4) Berry, R. S. *J. Chem. Soc., Faraday Trans.* **1990**, *86*, 2343.

(5) Labastie, P.; Whetten, R. L. *Phys. Rev. Lett.* **1990**, 65 1567.

(6) Wales D. J.; Berry, R. S. *Phys. Rev. Lett.* **1994**, *73*, 2875.

(7) Wales, D. J.; Doye, J. P. K. *J. Chem. Phys* **1995**, *103*, 3061.

(8) Bösiger, J.; Leutwyler, S. *Phys. Rev. Lett.* **1987**, *59*, 1895.

(9) D. Eichenauer, D.; Le Roy, R. J. *Phys. Rev. Lett.* **1986**, *57*, 2920. Eichenauer, D.; Le Roy, R. J. *J. Chem. Phys.* **1988**, *88*, 2898.

(10) Bartell, L. S.; Dulles, F. J.; Chuko, B. *J. Phys. Chem.* **1991**, *95*, 6481. Bartell, L. S.; Xu, S. *J. Phys. Chem.* **1991**, *95*, 8939. Bartell, L. S. *J. Phys. Chem.* **1992**, *96*, 108.

(11) Fried, L. E.; Mukamel S. *Phys. Rev. Lett.* **1991**, *66*, 2340.

(12) Wales, D. J.; Ohmine, I. *J. Chem. Phys.* **1993**, 98, 7245.

(13) Buck, U.; Ettisher, I.; Melzer, M.; Buch, V.; Sadlej, J. *Phys. Rev. Lett.* **1998**, *80*, 2578.

(14) Gruenloh, C. J.; Carney, J. R.; Arrington, C. A.; Zwier, T. S.; Fredericks, S. Y.; Jordan, K. D. *Science* **1997**, *276*, 1679.

(15) For recent experimental evidences of the characteristics of stable structures in small aqueous clusters, see for example: Liu, K.; Brown, M. G.; Carter, C.; Saykally, R. J.; Gregory, J. K.; Clary, D. C. *Nature (London)* **1996**, *381*, 501. Gregory, J. K.; Clary, D. C.; Lui, K.; Brown, M. G.; Saykally, R. J. *Science* **1997**, *275*, 814. Liu, K.; Brown, M. G.; Cruzan, J. D.; Saykally, R. J. *J. Phys. Chem. A* **1997**, *101*, 9022. Liu, K.; Brown, M. G.; Saykally, R. J. *J. Phys. Chem. A* **1997**, *101*, 9011. Liu, K.; Brown, M. G.; Saykally, R. J. *J. Phys. Chem. A* **1997**, *101*, 8995.

(16) Rodriguez, J.; Laria, D.; Marceca, E. J.; Estrin, D. A. *J. Chem. Phys.* **1999**, *110*, 9039.

(17) Tsai, C. J.; Jordan, K. D. *J. Chem. Phys.* **1991**, *95*, 3850.

(18) Tsai, C. J.; Jordan, K. D. *J. Phys. Chem.* **1993**, *97*, 7245. Tsai, C. J.; Jordan, K. D. *J. Phys. Chem.* **1993**, *97*, 5208.

(19) Wales, D. J.; Ohmine, I. *J. Chem. Phys.* **1993**, *98*, 7257.

(20) Doye, J. P. K.; Wales, D. J. *J. Chem. Phys.* **1995**, *102*, 9673.

(21) Baba, A.; Hirata, Y.; Saito, S.; Ohmine, I.; Wales, D. J. *J. Chem. Phys.* **1997**, *106*, 3329.

(22) Wales, D. J.; Walsh, T. R. *J. Chem. Phys.* **1997**, *106*, 7193.

(23) Vegiri, A.; Farantos, S. C. *J. Chem. Phys.* **1993**, *98*, 4059.

(24) Masella, M.; Flament, J.-P. *J. Chem. Phys.* **1999**, *111*, 5081.

(25) Csajka, F. S.; Chandler, D. *J. Chem. Phys.* **1998**, *109*, 1125.

(26) Dellago, C.; Bolhuis, P. G.; Csajka, F.; Chandler, D. *J. Chem. Phys.* **1998**, *108*, 1964.

(27) Dellago, C.; Bolhuis, P. G.; Chandler, D. *J. Chem. Phys.* **1998**, *108*, 9263.

(28) Bolhuis, P. G.; Dellago, C.; Chandler, D. *Faraday Discuss. Chem. Soc.* **1998**, *110*, 421.

(29) Dellago, C.; Bolhuis, P. G.; Chandler, D. *J. Chem. Phys.* **1999**, *110*, 6617.

(30) Recent implementations of the transition path sampling algorithm can be found in: Geissler, P. L.; Dellago, C.; Chandler, D. *J. Phys. Chem. B* **1999**, *103*, 3706. Geissler, P. L.; Dellago, C.; Chandler, D. *Phys. Chem. Chem. Phys.* **1999**, *1*, 1317.

(31) For a recent review on constrained dynamics methods applied to computation of rate constants, see: Ciccotti G.; Ferrario, M. In *Classical and Quantum Dynamics in Condensed Phase Simulations*; Berne, B. J., Ciccotti, G., Coker, D. F., Eds.; World Scientific: Singapore, 1998; Chapter 7.

(32) Allen, M.; Tildesley, D. J. *Computer Simulations of Liquids*; Clarendon: Oxford, UK, 1987.

(33) Jorgensen, W. L.; Chandrasekhar, J., Madura, J. D.; Impey, R. W.; Klein, M. L. *J. Chem. Phys.* **1983**, *79*, 926.

(34) Andersen, H. C. *J. Comput. Phys.* **1983**, *52*, 24.

(35) Kim, J.; Mhin, B. J.; Lee, S. J.; Kim, K. S. *Chem. Phys. Lett.* **1994**, *219*, 243. Estrin, D. A.; Paglieri, L.; Corongiu, G.; Clementi, E. *J. Phys. Chem.* **1996**, *100*, 8701.

(36) The TIP4P model fails to reproduce this trend; however, for the present purposes this discrepancy is unimportant.